

Constrained Control Allocation Improving Fault Tolerance of a Four Wheel Independently Driven Articulated Vehicle

ALEXANDER SEIFFER¹, LUKAS SCHÜTZ^{1,2}, MICHAEL FREY³, AND FRANK GAUTERIN³

¹SHARE at KIT, Schaeffler Technologies AG & Co. KG., 76131 Karlsruhe, Germany

²Vehicle Dynamics and Redundancy, Knorr-Bremse Systeme für Nutzfahrzeuge GmbH, 71701 Schwieberdingen, Germany

³Institute of Vehicle System Technology, Karlsruhe Institute of Technology, 76131 Karlsruhe, Germany

CORRESPONDING AUTHOR: A. SEIFFER (e-mail: alexander.seiffer@schaeffler.com)

This work was supported by the KIT-Publication Fund of the Karlsruhe Institute of Technology.

ABSTRACT In articulated vehicles steering is accomplished by adjusting the articulation angle. Commonly a steering actuator is used to pivot the two vehicle sections. This actuator can be dispensed with if the pivoting is controlled by selective distribution of the drive torques to the individually driven wheels instead. Since steering is a safety-critical function, it must be ensured even if one of the drive motors fails. For this purpose, we propose a control method for a fault-tolerant four wheel independently driven articulated vehicle. The control method was developed and tested in a simulation environment and validated on a 1:5 scale demonstrator vehicle. The proposed method with constrained control allocation maintains the desired velocity and articulation angle by distributing the driving torques to the four wheels considering the current actuator limits. Both the simulation and the vehicle tests show that the control method meets the control objectives even when a sudden actuator limit occurs during critical driving scenarios like cornering. Thus, the vehicle can keep its maneuverability in the event of a detected failure of a drive motor. Together with reliable failure detection, the proposed approach provides a basis for further development towards innovative fault-tolerant electric articulated vehicles that meet the requirements of functional safety.

INDEX TERMS Articulated vehicle, chassis control, control allocation, drive-by-wire, fault tolerance, over-actuated vehicle, redundancy, resilience, steer-by-wire, vehicle dynamics control, wheel-individual drive.

I. INTRODUCTION

ELECTRIFICATION and automation are two major current development trends not only in the entire mobility sector but also regarding commercial vehicles [1]. An exemplary application for electric articulated vehicles are innovative sweepers [2], a use case that is also of interest in terms of automation [3]. In mining industry automated articulated haulers are a preferred solution, as articulated steering offers enhanced maneuverability [4] while automation increases safety of human operators [5].

The review of this article was arranged by Associate Editor Pardis Khayyer.

Drive-by-wire systems including steer-by-wire enable the deployment of automated driving functions. For lateral guidance the steer-by-wire control unit receives the steering commands from an input module and transmits the corresponding signals to an actuator that is connected to the steering gear module of the vehicle [6]. The steering command can come either from an operator interface (steering wheel) or, in the case of an automated driving vehicle, from a control unit [6], [7].

Unlike conventional steering systems, there is no mechanical link between the driver's input device and the steered wheels. Thus, the driver can no longer intervene as a fallback in the event of a malfunction of the steering actuation [6].

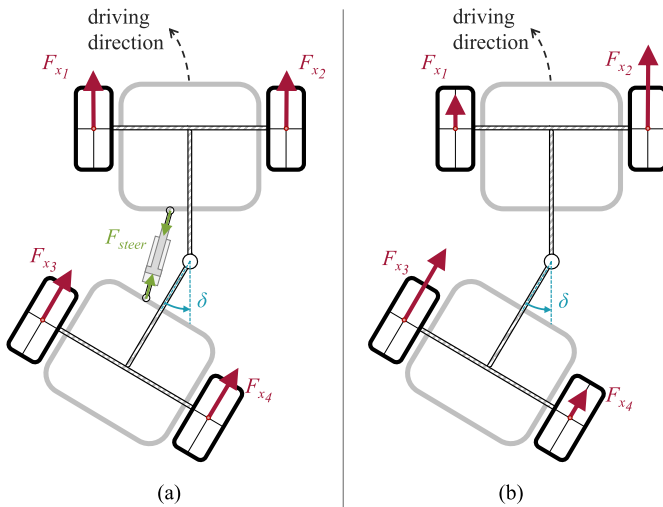


FIGURE 1. Actuator forces for longitudinal and lateral control of an articulated vehicle. (a) In conventional solutions longitudinal wheel forces F_{x1} – F_{x4} accelerate and decelerate the vehicle while the steering actuator (F_{steer}) adjusts the articulation angle δ . (b) An alternative concept uses the individually distributed wheel forces F_{x1} – F_{x4} for both longitudinal and lateral control by means of differential steering [10]. In the considered case, forces F_{x2} and F_{x4} are increased compared to F_{x1} and F_{x3} , which causes the front vehicle section to experience counterclockwise torque and the rear section to experience clockwise torque, resulting in a change in the articulation angle δ .

The requirements for fault-tolerant steer-by-wire systems towards reliability and availability, both in manual operated and automated vehicles, are therefore very demanding [7], [8]. Classically, these requirements are met by using hardware redundancies, but there are alternative approaches, such as the architecture presented by Bergmiller [9], which reduces the need for hardware redundancies by exploiting vehicle-wide functional redundancies.

Articulated vehicles are steered by pivoting the two vehicle sections. Commonly a hydraulic actuator is used to adjust the articulation angle δ (Fig. 1a) [11]. In the course of the electrification of articulated vehicles, hydraulic systems are replaced by electric drives and actuators, whereby the steering actuator is usually still designed as a hydraulic actuator [2], [12]. To reduce the energy consumption of the hydraulic steering system Xu et al. [13] proposed an assist-steering method based on drive-torque distribution (skid steering or differential steering) and obtained a reduction of the steering actuator force for about 41.2%.

The use of differential steering in articulated vehicles not only enables the reduction of actuator load but also the complete substitution of the steering actuator (Fig. 1b). Lateral and longitudinal dynamics of the vehicle are controlled by distributing the longitudinal wheel forces F_{x1} – F_{x4} to the four individually driven wheels. This approach investigated by Wadephul et al. [10] enables full electrification of an articulated vehicle without hydraulic components.

In order to make this type of steering actuation usable as steer-by-wire system in manually or autonomous driven articulated vehicles, it is necessary to ensure the vehicles



FIGURE 2. Demonstrator vehicle (scale 1:5) consisting of the front vehicle section (right) and the rear section (left). The sections are connected with an articulated swivel joint that is freely rotatable around the articulation axis and the longitudinal axis. The vehicle measures 920 mm in length and 375 mm in width and has a maximum articulation angle δ of 50°. The vehicle is driven by four electric motors (82 W per wheel).

functionality even in the event of a drive motor failure. For this purpose we propose a vehicle dynamics control approach for a four wheel individually driven articulated vehicle in this paper. The approach allows for compensation of the effect of a drive motor failure on the vehicles maneuverability.

For the investigation and development of the vehicle dynamics control a demonstrator vehicle (scale 1:5) was used (Fig. 2). In addition we set up a simulation model with the software tool MATLAB representing the vehicle dynamics of the demonstrator. The function of the proposed control approach is to follow the desired setpoints (vehicle velocity v_{sp} and articulation angle δ_{sp}) by adjusting the four control variables (drive torques M_{D1} – M_{D4}) taking into account current actuator limits or failures. We developed the control approach based on the simulation model and tested it with defined driving maneuvers in combination with emulated actuator failures. To validate the results gained with the simulation model and to prove the functionality of the approach on a real vehicle we have carried out test drives with the demonstrator vehicle.

This paper is organized as follows: Section II introduces the methodology of this work, including the description of the demonstrator vehicle, the corresponding vehicle dynamics model, and the maneuvers used for testing and validation. In Section III we describe the reference control method and the proposed control method with constrained control allocation. The results of the driving tests of the simulation-based study and those of the demonstrator vehicle tests are presented and discussed in Section IV, followed by the conclusion in Section V.

II. METHODS AND PROCEDURES

A. DEMONSTRATOR VEHICLE

The demonstrator vehicle is an electric four wheel independently driven articulated vehicle, that is not equipped with any steering actuator (Fig. 2). It can be controlled manually via remote control, controlling articulation angle δ and driving force F_{Drive} . In automated mode, it follows an offline defined time sequence of articulation angle δ and vehicle velocity v .

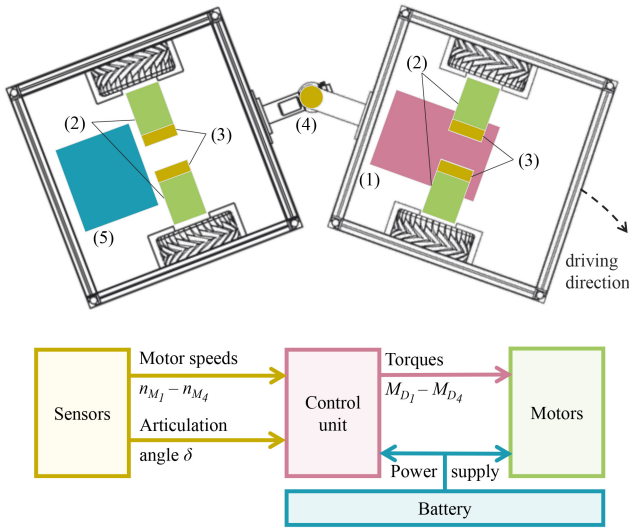


FIGURE 3. Placement of the main components within the demonstrator vehicle (top) and functional diagram (bottom): control unit (1), electric motor and gear units with motor controllers (2), motor speed sensors (3), articulation angle sensor (4) and battery (5).

Sensors, motors, motor controllers, control unit and battery are the essential components of the mechatronic system (Fig. 3). The controller approach developed in the simulation environment (MATLAB) can be compiled and transferred to the control unit of the vehicle. The motor speeds $n_{M1}-n_{M4}$ and the articulation angle δ are available to the controller as measured input variables. The drive torques $M_{D1}-M_{D4}$ are defined as output variables and result in the driving forces $F_{D1}-F_{D4}$.

B. VEHICLE DYNAMICS SIMULATION MODEL

The articulated vehicle is a multi-body system consisting of two bodies. We used a free body diagram of vehicle sections to find the system equations (Fig. 4). Assumptions and simplifications were made in order to set up the system equations. Due to the low height of the center of gravity and the low lateral acceleration, the vehicle can be assumed to be flat and weight transfer can be neglected. The lateral wheel forces $F_{y1}-F_{y4}$ can be assumed to increase linearly with the corresponding lateral slip angles $\alpha_1-\alpha_4$, and the cornering stiffnesses $c_{1,2}$ at the front axle and $c_{3,4}$ at the rear axle are constant accordingly. There is no consideration of longitudinal slip, instead longitudinal wheel forces $F_{x1}-F_{x4}$ are calculated directly as resultant forces from the driving forces $F_{D1}-F_{D4}$ and the wheel and gear resistance forces F_R . The functionality of the articulation joint J is represented by the joint forces R_x and R_y and the joint damping torque M_d .

The coordinate systems of the vehicle sections are placed in the corresponding centers of gravity CG_1 and CG_2 . The vehicle has four degrees of freedom, which are the minimal coordinates to describe the free dynamics of the system. These minimal coordinates correspond to the state variables of the model. They are the longitudinal velocity \dot{x}_1 (which

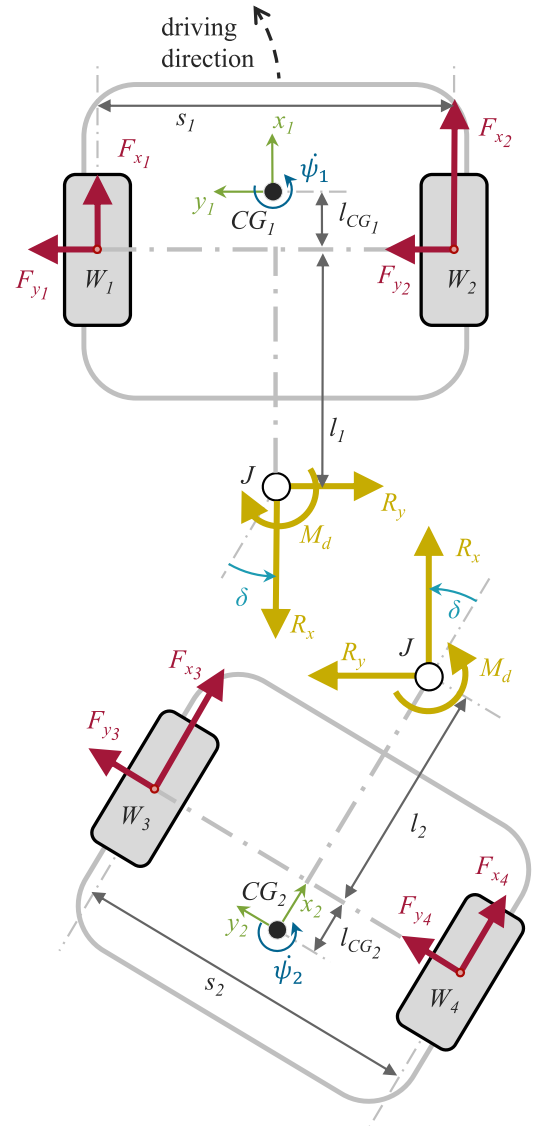


FIGURE 4. Free body diagram of the two body system representing the demonstrator vehicle with longitudinal wheel forces $F_{x1}-F_{x4}$ and lateral wheel forces $F_{y1}-F_{y4}$, joint forces R_x and R_y , damping torque M_d , articulation angle δ , yaw rate of the front section ($\dot{\psi}_1$) and the rear section ($\dot{\psi}_2$), coordinate system of the front section (x_1, y_1) and the rear section (x_2, y_2). All other parameters of the vehicle model are listed in Table 3.

is defined as vehicle velocity v), the lateral velocity \dot{y}_1 and the yaw rate $\dot{\psi}_1$ of the front vehicle section as well as the articulation angle δ . All other quantities like the velocities and the yaw rate of the rear vehicle section and the lateral slip angle $\alpha_1-\alpha_4$ can be calculated at any time from these four state variables.

To derive the total system equation, all necessary components first need to be set up in the corresponding coordinate systems. Then they can be transformed into the front section coordinate system to evaluate the equilibrium conditions. For the detailed derivation, refer to Appendix A. The six scalar equations of the equilibrium conditions resulting from (46)–(49) have to be solved according to the highest order

derivatives of the four state variables by eliminating the internal forces R_x and R_y . This can be done with MATLAB using the command *solve* in symbolic notation. Finally, these four equations are obtained:

$$\begin{aligned}\ddot{x}_1 &= f_1(\dot{x}_1, \dot{y}_1, \dot{\psi}_1, \delta, \dot{\delta}, F_{D_1}, F_{D_2}, F_{D_3}, F_{D_4}) \\ \ddot{y}_1 &= f_2(\dot{x}_1, \dot{y}_1, \dot{\psi}_1, \delta, \dot{\delta}, F_{D_1}, F_{D_2}, F_{D_3}, F_{D_4}) \\ \ddot{\psi}_1 &= f_3(\dot{x}_1, \dot{y}_1, \dot{\psi}_1, \delta, \dot{\delta}, F_{D_1}, F_{D_2}, F_{D_3}, F_{D_4}) \\ \ddot{\delta} &= f_4(\dot{x}_1, \dot{y}_1, \dot{\psi}_1, \delta, \dot{\delta}, F_{D_1}, F_{D_2}, F_{D_3}, F_{D_4})\end{aligned}\quad (1)$$

To set up a first-order state-space representation, the states are substituted as follows:

$$\begin{aligned}z &= [\dot{x}_1 \quad \dot{y}_1 \quad \dot{\psi}_1 \quad \delta \quad \dot{\delta}]^T \\ u &= [F_{D_1} \quad F_{D_2} \quad F_{D_3} \quad F_{D_4}]^T\end{aligned}\quad (2)$$

The first order nonlinear state-space representation results in

$$\dot{z} = f(z, u) \quad z(0) = z_0 \quad (3)$$

By solving these differential equations, the states of the system can be calculated for given initial conditions and trajectories of the control variables u , which allows for the simulation of the vehicle behavior.

C. TEST AND VALIDATION PROCEDURE

We used two different maneuvers to evaluate the control approach. During the test run, a failure of a drive could be initiated to consider how the vehicle compensates for the failure. We ran each test with both the proposed approach and, to provide a benchmark for evaluation, additionally with a reference control approach as used by Wadehul et al. [10]. First, we performed the investigations on the simulation model and then validated the results in selected aspects on the real vehicle.

The first maneuver was a step-steer followed by a steady-state circular maneuver. We used it to investigate how the behavior of the vehicle differs during a step in the articulation angle setpoint, depending on whether a failure of a drive is present or not. In a further test, the failure was initiated later during the steady-state circular drive. From this, the immediate response of the control approach to a failure could be evaluated.

In addition, a slalom maneuver was considered. Compared to the first maneuver, the required articulation angle in this case changes continuously, making this maneuver suitable for investigating the dynamic steering behavior before, during and after a failure. This allowed us to evaluate the vehicle's driving behavior in critical situations such as a drive failure during an evasive maneuver.

In the following, the maneuvers, failure scenarios and the quantities that were evaluated are considered in more detail.

1) DRIVING MANEUVERS

The step-steer maneuver included a short acceleration phase while driving straight and a step in the articulation angle

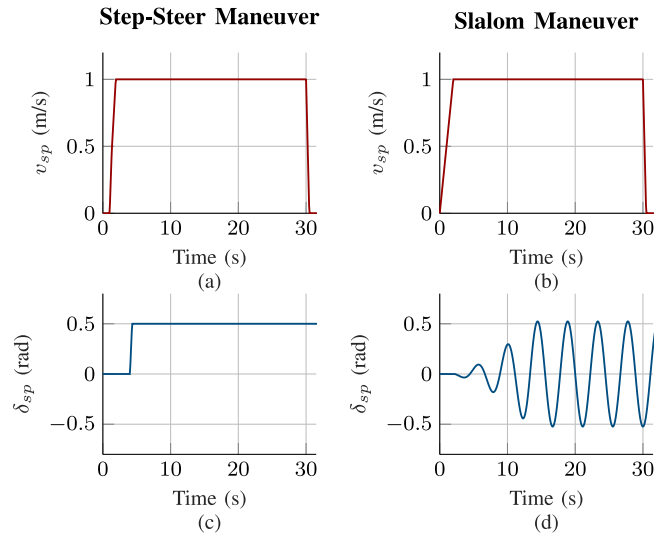


FIGURE 5. Setpoints. (a) Vehicle velocity v_{sp} for the step-steer maneuver. (b) Vehicle velocity v_{sp} for the slalom maneuver. (c) Articulation angle δ_{sp} for the step-steer maneuver. (d) Articulation angle δ_{sp} for the slalom maneuver.

setpoint after 4 s followed by stationary circular maneuver at constant velocity. At the end of the maneuver, a braking process was initiated at a constant articulation angle.

In order for the maneuver to be considered both demanding and representative of a real driving situation, the speed and articulation angle specifications are chosen in consideration of the step-steer definition of ISO 7401 [14]. There, a lateral acceleration of 4 m/s² is recommended. Taking into account the vehicle scale, a lateral acceleration of at least 0.8 m/s² is therefore required.

We choose a vehicle velocity v_{sp} of 1 m/s and an articulation angle δ_{sp} of 0.5 rad (which equals approximately 29°) resulting in a turn radius of about 1 m, a yaw rate $\dot{\psi}_1$ of about 1 rad/s and a lateral acceleration of 1 m/s², which makes the maneuver exceeding the requirements of the ISO 7401.

The slalom maneuver also started with straight line acceleration phase. After reaching constant velocity the articulation angle setpoint δ_{sp} was defined by a sine function with frequency of 0.225 Hz while the amplitude was slowly increased within 10 s to its maximum value of 0.5236 rad (30°).

The course of the vehicle velocity v_{sp} and articulation angle δ_{sp} setpoints is illustrated in Fig. 5.

2) FAILURE SCENARIOS

The failures of each of the four drives were considered separately. A failure was emulated by overwriting the corresponding drive torque M_{D_i} with 0 Nm. In the case of the step-steer maneuvers, the failure was initiated either from the beginning or during the stationary circular maneuver. The failure during the slalom maneuver was initiated at the moment of the highest steering torque demand, which enables a worst-case consideration.

TABLE 1. Experimental plan comprising maneuver and failure scenario.

No.	Maneuver	Control method	Failure scenario
1.1	Step-steer	Reference	None
1.2	Step-steer	Proposed method	None
2.1	Step-steer	Reference	W_1 at $t = 0$ s
2.2	Step-steer	Proposed method	W_1 at $t = 0$ s
3.1	Step-steer	Reference	W_1 after step-steer ($t = 12$ s)
3.2	Step-steer	Proposed method	W_1 after step-steer ($t = 12$ s)
4.1	Step-steer	Reference	W_2 after step-steer ($t = 12$ s)
4.2	Step-steer	Proposed method	W_2 after step-steer ($t = 12$ s)
5.1	Step-steer	Reference	W_3 after step-steer ($t = 12$ s)
5.2	Step-steer	Proposed method	W_3 after step-steer ($t = 12$ s)
6.1	Step-steer	Reference	W_4 after step-steer ($t = 12$ s)
6.2	Step-steer	Proposed method	W_4 after step-steer ($t = 12$ s)
7.1	Slalom	Reference	W_1 mid-maneuver ($t = 15.9$ s)
7.2	Slalom	Proposed method	W_1 mid-maneuver ($t = 15.9$ s)

3) ANALYSIS

The following values were recorded for the evaluation of the experiments: actual articulation angle δ_{act} , actual velocity v_{act} , steering controller output M_{Steer} and drive torques $M_{D_1}-M_{D_4}$.

To quantitatively compare the performance of the two approaches, error metrics were applied to the evaluation intervals of interest. The maximum absolute deviation of the actual articulation angle from its setpoint is given by $\hat{\delta}_{error}$, while δ_{RMSE} is the root-mean-square error of the articulation angle deviation.

4) RESULTING EXPERIMENTAL PLAN

From preliminary tests with the reference method, we knew that with a positive articulation angle, the failure of the drive at the front left wheel (W_1) is the most difficult failure to compensate, since it leads to the largest control deviations compared to failures of drives at other wheels. Therefore, mainly the failure of the drive at wheel W_1 is considered. However, for the scenario of a sudden failure during a stationary circular maneuver, the experimental plan also includes the failures of the drives of the other wheels to evaluate how they affect the compensation behavior of the proposed method.

The combination of driving maneuvers, failure scenarios, and control methods considered in this work resulted in the experimental plan shown in Table 1.

III. CONTROL METHODS

The vehicle considered has four independently driven wheels and is thus overactuated, since two drives on one axle are already sufficient to follow the setpoints of vehicle velocity v_{sp} and articulation angle δ_{sp} (Fig. 1b).

In a four wheel driven articulated vehicle, the available degrees of freedom can thus be used to distribute the drive torques $M_{D_1}-M_{D_4}$ without unintentionally influencing the controlled process variable vehicle velocity v_{act} and articulation angle δ_{act} .

From this consideration, we concluded that a failure of a drive can be compensated immediately and completely

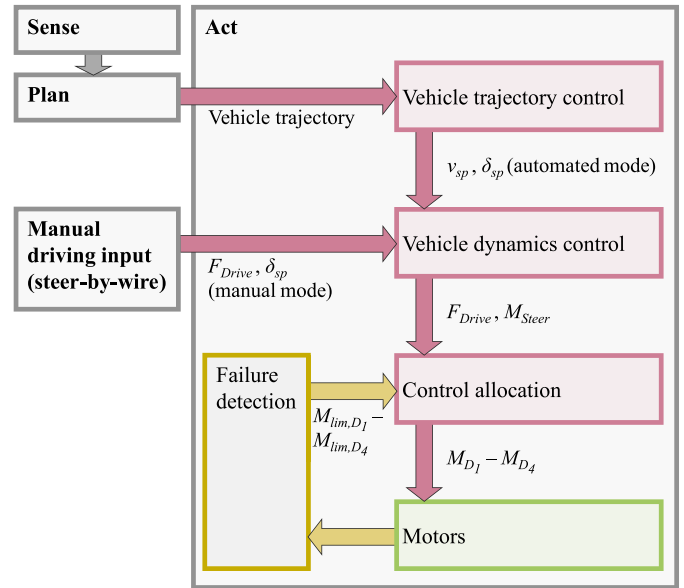


FIGURE 6. Integration of constrained control allocation and failure detection into the control method of an automated four wheel driven articulated vehicle.

by suitable redistribution of the drive torques $M_{D_1}-M_{D_4}$ by means of control allocation.

In the following, a constrained control allocation module is presented which we added to the existing controller to provide a fault-tolerant control method. Its task is to compensate for the failure of a drive motor in such a way that the vehicle continues to drive without failure-induced deviation of velocity v_{act} and articulation angle δ_{act} .

A. CONCEPT OF THE PROPOSED CONTROL METHOD

The proposed vehicle dynamics control with constrained control allocation was designed to be integrated into the overall vehicle control method of a steer-by-wire or an automated controlled articulated vehicle. A corresponding overall vehicle control structure is shown in Fig. 6. The automation function is based on the sense-plan-act paradigm [15], commonly used for automated driving.

The vehicle trajectory controller realizes the planned motion of the trajectory by specifying the vehicle velocity v_{sp} and articulation angle δ_{sp} . These are controlled in the vehicle dynamics controller by setting the total drive force F_{Drive} and the steering torque M_{Steer} . In manual driving mode, M_{Steer} is set by the vehicle dynamics controller based on the driver's steering angle input δ_{sp} , whereas the total drive force F_{Drive} is determined directly by the driver.

The total drive force F_{Drive} and the steering torque M_{Steer} serve as input variables for the control allocation module. It resolves the overactuation by deriving the four drive torques (actual controls) $M_{D_1}-M_{D_4}$ from the two control objectives (M_{Steer}, F_{Drive}).

In addition to the main purpose, the fulfillment of the control objectives, the remaining degrees of freedom of the drive

torque distribution can be used for the optimization of a secondary objective by setting up an optimization problem [16]. Minimizing energy or maximizing driving safety by reducing the maximum driving force of the four wheels are two possible applications.

The constrained control allocation must take into account the limitations of the drive torques $M_{lim,D_1}-M_{lim,D_4}$ when distributing the drive torques. In the fault-free case, the limitations correspond to the nominal drive torque (2.2 Nm). If the failure of a drive is detected by the failure detection, this limitation is communicated to the constrained control allocation module and taken into account. This results in a distribution of the drive torques which fulfills the control action of the controller without the use of the defective drive.

In the overall architecture shown, the vehicle dynamics control with control allocation can be understood as the inner control loop and the trajectory control (either conducted by the driver or by the controller of the automated function) as the outer control loop. The proposed method takes the approach of addressing the fault-tolerant functionality in this inner control loop to prevent the outer control loop from being affected in case of a drive failure. Therefore, the evaluation of the fault-tolerant behavior in this work is based on the control error of the inner control loop (articulation angle δ and vehicle velocity v).

B. REFERENCE CONTROL METHOD

The controller used by Wadephul et al. [10] was implemented as a reference. Velocity and articulation angle are each controlled in an independent PI and PID controller. In contrast to the control method proposed in Fig. 6, the control allocation approach of this reference control method does not consider constraints of the drive torques. Instead, the allocation problem is solved by specifying the following heuristic relations between the actuator torques and thus eliminating the degrees of freedom:

$$\begin{aligned} M_{D_3} &= M_{D_2} = M_{D_{2,3}} \\ M_{D_4} &= M_{D_1} = M_{D_{1,4}} \end{aligned} \quad (4)$$

To find the mapping between the actual controls ($M_{D_1}-M_{D_4}$) and the control objectives (M_{Steer}, F_{Drive}) further assumptions are made:

- F_{Drive} is the sum of the four drive torques divided by the dynamic wheel radius r_W .
- With their respective lever arm, the two driving forces of an axle generate a torque about the articulated joint axis. The sum of both torques (taking into account the direction of action) results in the steering torque M_{Steer} . The lever arms correspond to half the track width $s_{1,2}$ (Fig. 4).

As for the demonstrator vehicle the track widths of both sections are equal we define the overall steering lever arm r_S

$$r_S = 2s_1 = 2s_2 \quad (5)$$

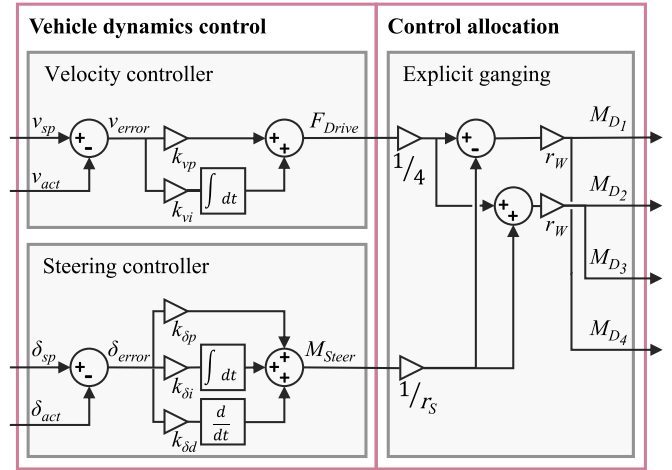


FIGURE 7. Reference control method with PID-controllers for velocity and steering control with explicit ganging control allocation based on [10].

With the dynamic wheel radius r_W we get

$$\begin{aligned} M_{D_{1,4}} &= r_W \left(\frac{1}{4} F_{Drive} - \frac{1}{r_S} M_{Steer} \right) \\ M_{D_{2,3}} &= r_W \left(\frac{1}{4} F_{Drive} + \frac{1}{r_S} M_{Steer} \right) \end{aligned} \quad (6)$$

This approach can also be described according to the explicit ganging method summarized by Oppenheimer et al. [16]. The control allocation problem can be formulated as

$$\mathbf{B}\boldsymbol{\delta} = \mathbf{d}_{des} \quad (7)$$

with

$$\begin{aligned} \boldsymbol{\delta} &= [M_{D_1} \quad M_{D_2} \quad M_{D_3} \quad M_{D_4}]^T \\ \mathbf{d}_{des} &= [F_{Drive} \quad M_{Steer}]^T \\ \mathbf{B} &= \frac{1}{r_W} \begin{bmatrix} 1 & 1 & 1 & 1 \\ -\frac{1}{4}r_S & \frac{1}{4}r_S & \frac{1}{4}r_S & -\frac{1}{4}r_S \end{bmatrix} \end{aligned} \quad (8)$$

where $\boldsymbol{\delta}$ is the control vector, \mathbf{d}_{des} the control objective vector and \mathbf{B} the control effectiveness matrix.

The ganging law becomes

$$\boldsymbol{\delta} = \mathbf{G}\boldsymbol{\delta}_{pseudo} \quad (9)$$

with

$$\begin{aligned} \boldsymbol{\delta}_{pseudo} &= [M_{D_{1,4}} \quad M_{D_{2,3}}]^T \\ \mathbf{G} &= \begin{bmatrix} 1 & 0 & 0 & 1 \\ 0 & 1 & 1 & 0 \end{bmatrix}^T \end{aligned} \quad (10)$$

Solving

$$\mathbf{B}\mathbf{G}\boldsymbol{\delta}_{pseudo} = \mathbf{d}_{des} \quad (11)$$

for the pseudo controls $\boldsymbol{\delta}_{pseudo}$ finally yields (6) again.

The resulting control method with the two controllers and the control allocation is shown in Fig. 7.

Tuning of the controller parameters on the demonstrator vehicle yielded $K_{Pv} = 40.4$, $K_{Iv} = 20.2$, $K_{P\delta} = 2.23$,

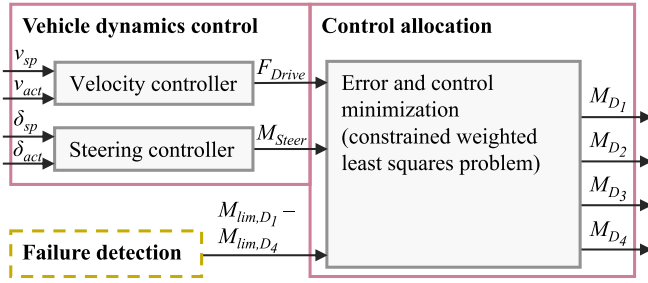


FIGURE 8. Proposed control method with constrained control allocation.

$K_{I\delta} = 2.58$ and $K_{D\delta} = 1.43$. The parameters found on the real vehicle were also chosen for the controllers in the simulation model.

C. PROPOSED CONTROL METHOD

The proposed controller approach (see Fig. 8) differs from the reference solution with respect to the control allocation method used. Velocity and steering controllers are not modified. The fault-tolerant behavior of the proposed solution is taken into account by considering the drive torques limits $M_{lim,D1}-M_{lim,D4}$ obtained from the failure detection module. For this purpose, an iterative constraint optimization method is chosen. Again the control allocation problem can be described according to equation (7) with

$$\begin{aligned} \delta &= [M_{D1} \quad M_{D2} \quad M_{D3} \quad M_{D4}]^T \\ \mathbf{d}_{des} &= [F_{Drive} \quad M_{Steer}]^T \\ \mathbf{B} &= \frac{1}{r_W} \begin{bmatrix} 1 & 1 & 1 & 1 \\ -r_{S_l} & r_{S_r} & r_{S_l} & -r_{S_r} \end{bmatrix} \end{aligned} \quad (12)$$

A consideration of the effect of driving forces on the steering torque M_{Steer} (see Appendix B) revealed that the steering lever arm r_S cannot be assumed to be constant, as it was in the reference approach. According to the consideration, the pseudo steering lever arms r_{S_r} and r_{S_l} for the wheels on the left and right side of the vehicle are described below as a function of the articulation angle.

$$\begin{aligned} r_{S_l} &= \frac{1}{2}s + l \tan\left(\frac{1}{2}\delta_{act}\right) \\ r_{S_r} &= \frac{1}{2}s - l \tan\left(\frac{1}{2}\delta_{act}\right) \end{aligned} \quad (13)$$

To solve the control allocation problem (7), it can be described as a mixed optimization problem according to Oppenheimer et al. [16] and Härkegård [17] with the objective to find a δ that minimizes

$$J = \|\mathbf{W}_\delta(\delta - \delta_p)\|^2 + \gamma \|\mathbf{W}_{des}(\mathbf{B}\delta - \mathbf{d}_{des})\|^2 \quad (14)$$

where δ_p is the preferred control vector and $\|\mathbf{u}\|^2 = \mathbf{u}^T \mathbf{u}$ (2-norm). \mathbf{W}_δ and \mathbf{W}_{des} are the weighting matrices and their elements are defined as

$$\begin{aligned} \mathbf{W}_\delta &= \text{diag}(W_{\delta_1}, \dots, W_{\delta_4}) \\ \mathbf{W}_{des} &= \text{diag}(W_{d_1}, W_{d_2}) \end{aligned} \quad (15)$$

A large value must be chosen for the weighting factor γ to achieve minimization of the control error rather than the control vector [17]. In the following we set $\gamma = 1$ and to achieve the required higher weighting of the second term relative to the first term in (14), we choose larger values for the elements of the weighting matrix \mathbf{W}_{des} compared to those of the weighting matrix \mathbf{W}_δ .

With

$$\delta_p = [0 \quad 0 \quad 0 \quad 0]^T \quad (16)$$

the optimal control vector δ_{opt} becomes

$$\delta_{opt} = \arg \min_{\underline{\delta} < \delta \leq \bar{\delta}} \|\mathbf{W}_\delta \delta\|^2 + \|\mathbf{W}_{des}(\mathbf{B}\delta - \mathbf{d}_{des})\|^2 \quad (17)$$

The vectors $\underline{\delta}$ and $\bar{\delta}$ contain the lower and upper bounds and with the drive torques limits $M_{lim,D1}-M_{lim,D4}$ they become

$$\begin{aligned} \underline{\delta} &= [-M_{lim,D1} \quad -M_{lim,D2} \quad -M_{lim,D3} \quad -M_{lim,D4}]^T \\ \bar{\delta} &= [M_{lim,D1} \quad M_{lim,D2} \quad M_{lim,D3} \quad M_{lim,D4}]^T \end{aligned} \quad (18)$$

The weighted least square problem (17) can be rewritten as in [17] and we get

$$\delta_{opt} = \arg \min_{\underline{\delta} < \delta \leq \bar{\delta}} \left\| \underbrace{\begin{bmatrix} \mathbf{W}_{des} \mathbf{B} \\ \mathbf{W}_\delta \end{bmatrix}}_A \delta - \underbrace{\begin{bmatrix} \mathbf{W}_{des} \mathbf{d}_{des} \\ \mathbf{0} \end{bmatrix}}_b \right\|^2 \quad (19)$$

Therefore, the formulation solving the overdetermined system becomes

$$\delta_{opt} = \arg \min_{\underline{\delta} < \delta \leq \bar{\delta}} \|\mathbf{A}\delta - \mathbf{b}\| \quad (20)$$

Since MATLAB is used for both simulation and code generation for the vehicle controller, we used the operator “\” (or *mldivide*) [18] to receive the unconstrained least-squares solution of (20) as

$$\delta_{opt,unconstr} = \mathbf{A} \setminus \mathbf{b} \quad (21)$$

The control constraints are considered by an iterative redistribution scheme based on the one of the redistributed pseudo inverse approach presented in [16]. The solution of the unconstrained system (21) is checked for compliance with the limits given in the constraint vectors $\underline{\delta}$ and $\bar{\delta}$. For the fault-free case the constraint vectors contain the nominal drive torques and in case of a failure the corresponding value is set to 0Nm. If at least one of the control values violates the constraints, the following steps are performed until all control values are within the constraint limits.

- 1) Set all control values $\delta(i)$ that violate the constraints to their corresponding limit value $\underline{\delta}(i)$ or $\bar{\delta}(i)$ respectively.
- 2) Define δ_{lim} containing all limited control values, the other elements are 0.
- 3) Reduce the control objective \mathbf{d}_{des} by the effect of the limited control values

$$\mathbf{d}_{des}^* = \mathbf{d}_{des} - \mathbf{B}\delta_{lim} \quad (22)$$

TABLE 2. Summary of the results of the simulation and the demonstrator vehicle test runs based on the two error metrics $\hat{\delta}_{error}$ and δ_{RMSE} . For the runs using the proposed method, the relative differences of the metrics with respect to the reference run are given in parentheses. For the test runs 1.1, 1.2, 2.1 and 2.2, two different intervals of the maneuver are evaluated.

Test run	Evaluation interval	Simulation		Demonstrator vehicle tests	
		$\hat{\delta}_{error}$ (rad)	δ_{RMSE} (rad)	$\hat{\delta}_{error}$ (rad)	δ_{RMSE} (rad)
1.1 (rm)	Entire maneuver	0.305	0.037	0.328	0.032
1.2 (pm)	Entire maneuver	0.307 (+1 %)	0.037 (0 %)	0.334 (+2 %)	0.032 (0 %)
1.1 (rm)	As of $t = 12$ s	0.023	0.005	0.039	0.011
1.2 (pm)	As of $t = 12$ s	0.023 (0 %)	0.005 (0 %)	0.022 (-44 %)	0.010 (-9 %)
2.1 (rm)	Entire maneuver	0.418	0.120	0.474	0.124
2.2 (pm)	Entire maneuver	0.309 (-26 %)	0.037 (-69 %)	0.311 (-34 %)	0.037 (-70 %)
2.1 (rm)	As of $t = 5$ s (1 s after step-steer)	0.296	0.078	0.474	0.106
2.2 (pm)	As of $t = 5$ s (1 s after step-steer)	0.079 (-73 %)	0.021 (-73 %)	0.071 (-85 %)	0.026 (-75 %)
3.1 (rm)	As of $t = 12$ s (failure at W_1)	0.296	0.120	0.439	0.130
3.2 (pm)	As of $t = 12$ s (failure at W_1)	0.020 (-93 %)	0.004 (-97 %)	0.031 (-93 %)	0.015 (-88 %)
4.1 (rm)	As of $t = 12$ s (failure at W_2)	0.146	0.042	0.147	0.058
4.2 (pm)	As of $t = 12$ s (failure at W_2)	0.022 (-85 %)	0.005 (-88 %)	0.041 (-72 %)	0.013 (-78 %)
5.1 (rm)	As of $t = 12$ s (failure at W_3)	0.373	0.101	0.285	0.099
5.2 (pm)	As of $t = 12$ s (failure at W_3)	0.028 (-92 %)	0.006 (-94 %)	0.033 (-88 %)	0.016 (-84 %)
6.1 (rm)	As of $t = 12$ s (failure at W_4)	0.116	0.034	0.117	0.043
6.2 (pm)	As of $t = 12$ s (failure at W_4)	0.020 (-83 %)	0.004 (-88 %)	0.039 (-67 %)	0.017 (-60 %)
7.1 (rm)	As of $t = 15.9$ s (failure at W_1)	0.613	0.336	-	-
7.2 (pm)	As of $t = 15.9$ s (failure at W_1)	0.399 (-35 %)	0.250 (-26 %)	-	-

- 4) Define B^* and W_δ^* by deleting all rows and/or columns in B and W_δ that correspond to an limited control value.
- 5) Solve the reduced least squares problem of the unconstrained controls

$$\delta_{opt}^* = \begin{bmatrix} W_{des} B^* \\ W_\delta^* \end{bmatrix} \setminus \begin{bmatrix} W_{des} d_{des}^* \\ \mathbf{0} \end{bmatrix} \quad (23)$$

- 6) Return the control vector δ_{opt} containing both constrained control values (δ_{lim}) and unconstrained control values (δ_{opt}^*)

The behavior of the constrained control allocation can be adjusted by the specification of the matrices W_δ and W_{des} . As mentioned above, it is important that the elements in W_{des} are significantly larger than those in W_δ . By selecting different sizes for the individual elements in W_δ , it is possible, for example, to distribute the drive torques preferentially to one of the vehicle axles. The specification of W_{des} can be used accordingly to prioritize the fulfillment of the two control objectives against each other. For the given application, we assumed that the fulfillment of the steering control is to be prioritized higher than that of the drive control, which is why $W_{d_1} < W_{d_2}$ was chosen. The tests considered in the simulation and on the demonstrator vehicle were performed with the following values: $W_{d_1} = 10$, $W_{d_2} = \sqrt{1500}$, $W_{\delta_1, \dots, 4} = \sqrt{2}$.

IV. RESULTS AND DISCUSSION

The results of the test runs both in the simulation and with the demonstrator vehicle are represented by uniform plots. For each test run considered, the measurements of the attempt using the reference method (index “rm”) and the proposed method (index “pm,”) are shown in a common plot. The quantities from top to bottom in the figure are: vehicle velocity v_{act} , articulation angle δ_{act} , steering torque M_{Steer} , wheel torques of the reference method $M_{D1,rm}-M_{D4,rm}$ and wheel torques of the proposed method $M_{D1,pm}-M_{D4,pm}$. The

resulting error metrics for each test run are summarized in Table 2. To illustrate the test drives of the demonstrator vehicle, they are documented in a video that can be accessed via [19].

A. STEP-STEER WITHOUT DRIVE FAILURE

Fig. 9 shows the result plots of the step-steer maneuver without drive failure (test runs 1.1 and 1.2) whereas the left column contains the results of the simulation and the right column those of the tests with the demonstrator vehicle.

The target velocity was reached after about 1 s followed by a small overshoot of 0.05 m/s in the simulation and 0.1 m/s on the demonstrator vehicle. In the simulation, the velocity was constant in the further course, while on the demonstrator vehicle a periodic oscillation around the setpoint value could be observed. The resulting velocity of the reference method and proposed method variants were identical. The period of the oscillation of the velocity corresponds to the duration of one round trip of the driven circle. We attribute the cause to the slightly tilted floor at the location of the test drives.

The demonstrator vehicle reached the target articulation angle 0.3 s after the setpoint signal and exceeded the setpoint value by 0.03 rad (1.7°) with the proposed method. In the further course and also during braking of the vehicle, the articulation angle remained constant with deviations smaller than 0.025 rad (1.4°). The articulation angle in the simulation showed a slower control response and an overshoot of 0.08 rad (4.6°) which was the largest deviation of the simulation from the demonstrator vehicle test results. We attribute this behavior to the fact that the controller parameters have been optimized for the demonstrator vehicle and the same parameters were used in the simulation. Due to deviations of the simulation model from reality, the controller in the simulation did not behave identically to the one of the demonstrator vehicle. The steering torque required for step steer was 2.1 Nm in the simulation and 2.3 Nm on

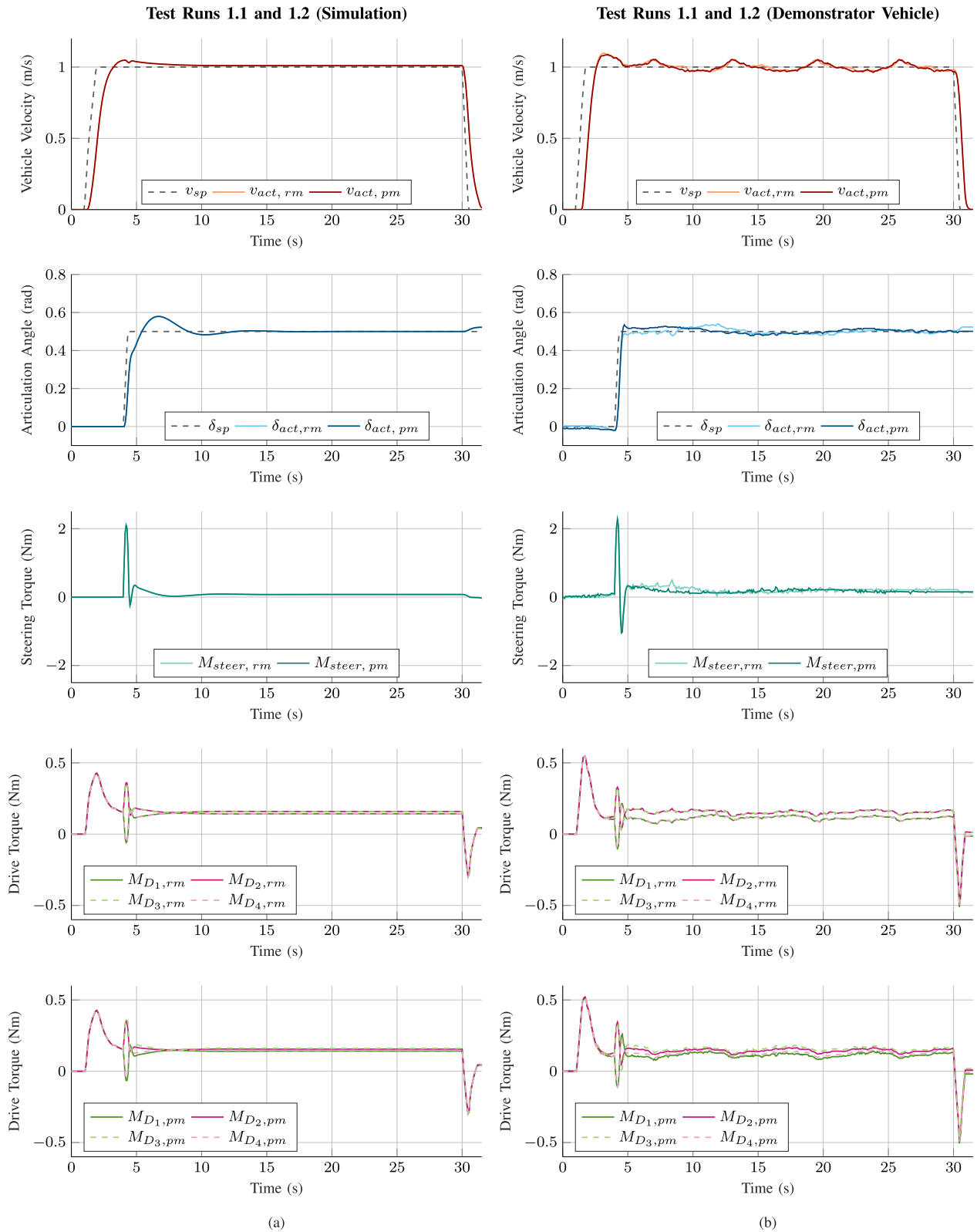


FIGURE 9. Results of the step-steer maneuvers without failure (test runs 1.1 and 1.2) for the two attempts with reference control method (rm) and proposed control method (pm). (a) Results from the simulation test runs. (b) Results from the demonstrator vehicle test runs.

the demonstrator vehicle. During continuous cornering, the steering torque required to maintain the articulation angle was approximately 0.1 Nm.

As expected from the torque distribution of the reference method, the drive torques of the diagonally opposite wheels were identical. During step-steer, negative drive torques were

applied at wheels W_1 and W_4 in order to generate the required steering torque. When the proposed method was used, comparable results were obtained, although different drive torques were applied after step-steer due to the different sizes of the pseudo lever arms of the four wheels. During the entire maneuver, none of the drives reached its maximum actuating torque of 2.2Nm, from which it can be concluded that no constraint violation occurred when solving the least square problem and thus no redistribution had to take place.

Overall, it can be said that the behavior of the demonstrator vehicle and the simulation model showed good compliance, apart from the behavior of the steering controller in the simulation as described above. On the demonstrator vehicle, the controllers successfully tracked the course of the set points, regardless of the control allocation selected (reference method or proposed method).

In the following the focus is on the demonstrator vehicle test results and the differences between the reference method and the proposed methods in context of drive failures.

B. STEP-STEER WITH DRIVE FAILURE

Using the reference control method (test run 2.1) a failure of drive the at the front left wheel resulted in unintended cornering with an articulation angle of 0.30 rad (17°) during the acceleration phase (Fig. 10). After the step-steer the articulation angle oscillated between 0.43 rad (25°) and 0.60 rad (34°). When the vehicle decelerated the articulation angle was reduced to 0.02 rad (1.1°).

With the proposed control method (test run 2.2), the vehicle could be held straight when accelerating. The step steer angle was achieved with an overshoot of 0.07 rad (4.0°), after which a decaying oscillation between 0.45 rad (26°) and 0.52 rad (30°) occurred. During braking, the articulation angle was kept constant. Compared to the reference method, the root-mean-square error δ_{RMSE} of the entire maneuver was reduced by 70% from 0.124 rad to 0.037 rad (Table 2).

The reference control method does not take the failed drive into account. The unrealized drive torque acts like an external disturbance which must be compensated by the controller. The controller reacts to the control deviation by increasing the control value (see curve $M_{steer,rm}$). However, the reaction is not that fast that an immediate compensation of the disturbance is possible. The disturbance effect of the failed actuator also influences the controller dynamics, so that even in the steady-state case the controller no longer has the same stability as without failure.

With the proposed control method, the drive failure is considered by setting the control value limitation for the failed actuator to 0Nm. This results in a violation of the unconstrained solution of the least squares problem and the redistribution is performed throughout the maneuver. Since none of the other actuators reach their maximum actuating torque, a single iteration of the redistribution always results in a valid solution.

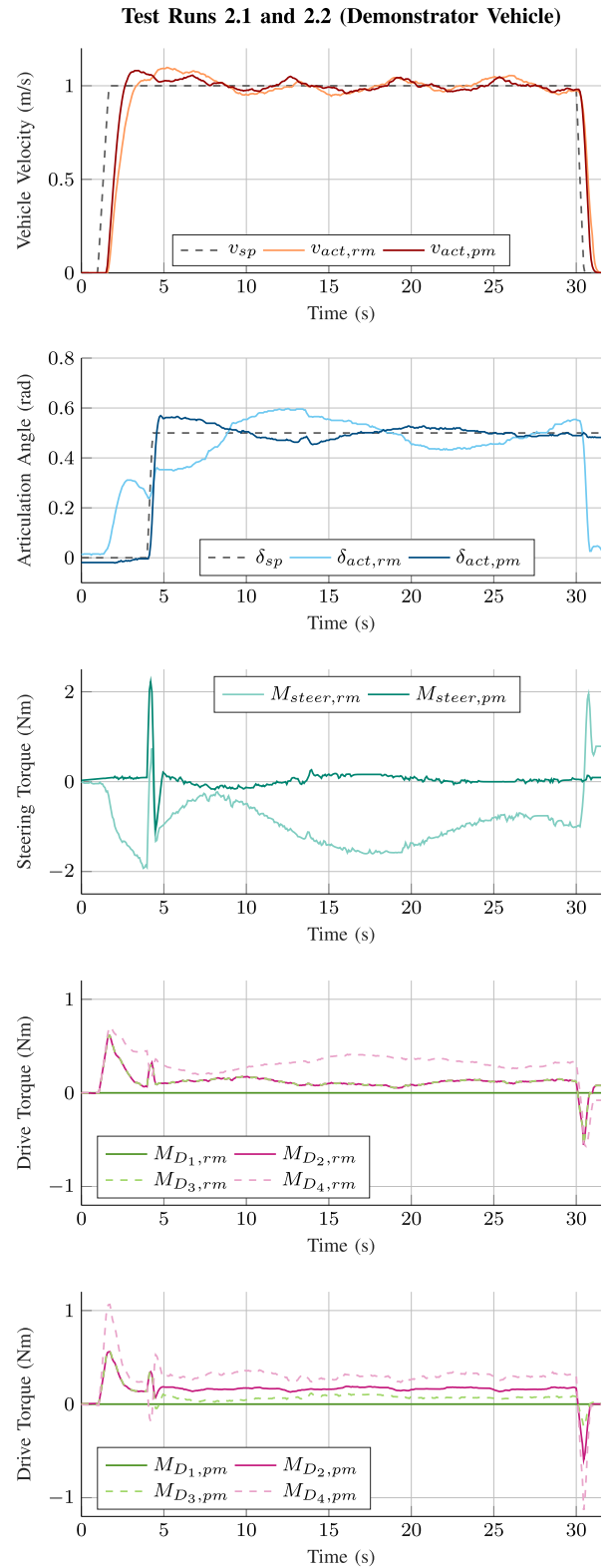


FIGURE 10. Results of the step-steer maneuvers with permanent failure of the front left drive from the demonstrator vehicle test runs 2.1 and 2.2, respectively for the two attempts with reference control method (rm) and proposed control method (pm).

The curve of the steering torque does not deviate significantly from the corresponding curve of test run 1.2 (step-steer without drive failure). We see this as a proof that the control

allocation redistributes the controller output despite the failed actuator in such a way that the desired effect of the controller output variable is achieved. The controller dynamics are thus preserved.

Compared to the other drive torques, the torque of the right rear wheel obtains the largest values during the maneuver. During acceleration, the maximum torque of this wheel, measuring 1.1 Nm, is twice as high as the drive torque of the other wheels.

With regard to lateral dynamics, the results provide information on the extent to which the system reaches its limits during this maneuver in the event of failure. At constant circular speed, the failure of the front left drive results in a maximum required drive torque at the rear right drive of 0.37 Nm, which corresponds to 17% of the drive torque capacity of 2.2 Nm.

More demanding than steady-state circular driving is the change of the articulation angle during the step steer. Here, the maximum drive torque is 0.53 Nm, which corresponds to 24% of the drive torque capability. Thus, it must be verified that the rate achieved meets the requirements in case of the failure. The ISO 7401 standard specifies a maximum steering wheel angle rate of 500°/s [14]. To apply this specification to an appropriate articulation angle rate of an articulated vehicle, we consider the duration required to reach the maximum steering angle from neutral position. Assuming a passenger car with 540° steering wheel angle difference from center to maximum steering wheel angle [20], a steering wheel angle rate of 500°/s corresponds to a duration of 1.08 s. Taking into account the maximum articulation angle of the articulated vehicle, this results in a corresponding maximum articulation angle rate requirement of 0.81 rad/s. From Fig. 10 it can be observed that the achieved articulation angle rate is 0.97 rad/s. From this we conclude that the selected maneuver exceeds the requirements for the step-steer specified in the ISO 7401 standard not only in terms of lateral acceleration (see Section II-C1), but also in terms of maximum steering rate. Yet the maximum drive torque of a single wheel reaches only 24% of its drive torque capacity. This indicates that with the proposed approach, higher lateral accelerations can be achieved without reaching the system limit, even in the case of a drive failure.

C. DRIVE FAILURE WHILE CORNERING

The evaluation of test runs 3.1 and 3.2 (Fig. 11) focuses on the period after the sudden failure of the drive. The results at the beginning of the maneuver were identical to the step-steer maneuver without failure (test runs 1.1 and 1.2) and the behavior at the end of the maneuver were similar to that of the step-steer with permanent drive failure (test runs 2.1 and 2.2). When using the reference control method, 4 s after the failure of the drive, the deviation of the articulation angle reaches 0.16 rad (9.2°). After that, oscillations occurred as in test run 2.1. Overall, the resulting root-mean-square error δ_{RMSE} for the evaluation interval after the drive failure is 0.130 rad.

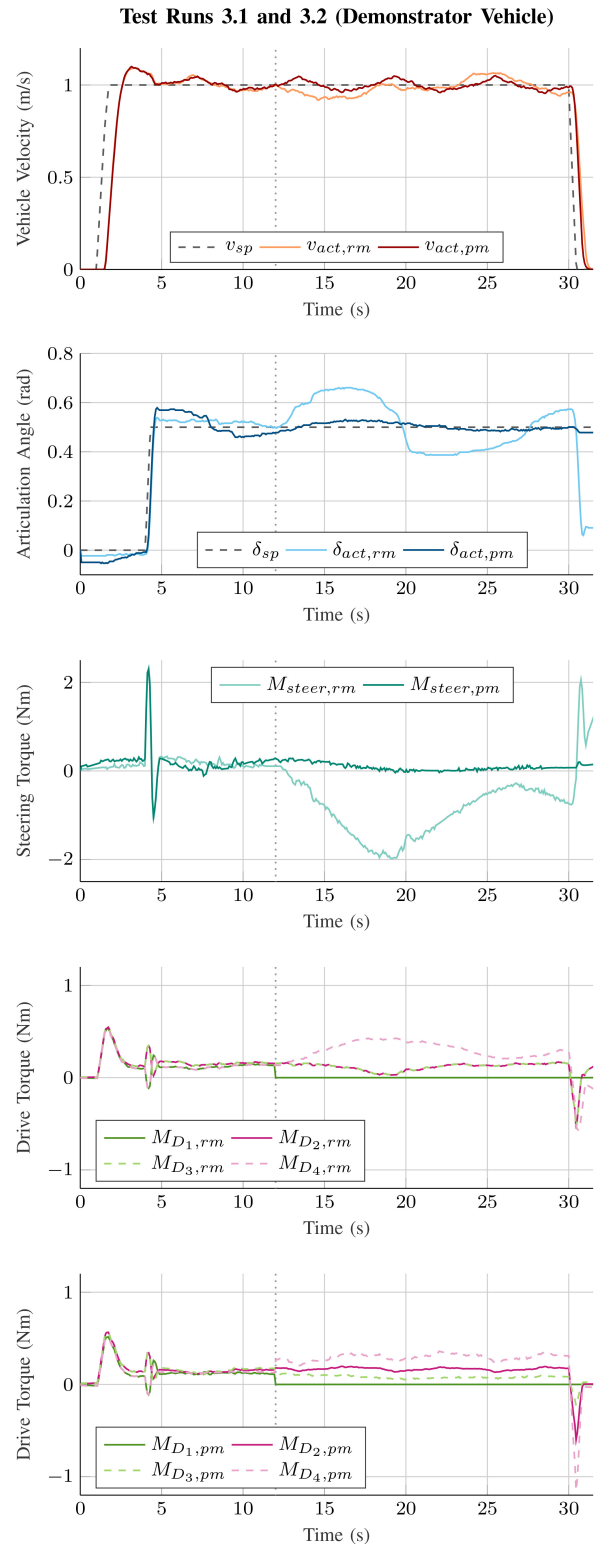


FIGURE 11. Results of the step-steer maneuvers with sudden failure of the front left drive at $t = 12$ s (indicated by dotted vertical line) from the demonstrator vehicle test runs 3.1 and 3.2, respectively for the two attempts with reference control method (rm) and proposed control method (pm).

The use of the proposed control method resulted in no failure-induced deviation of the articulation angle, and the resulting root-mean-square error δ_{RMSE} was reduced to

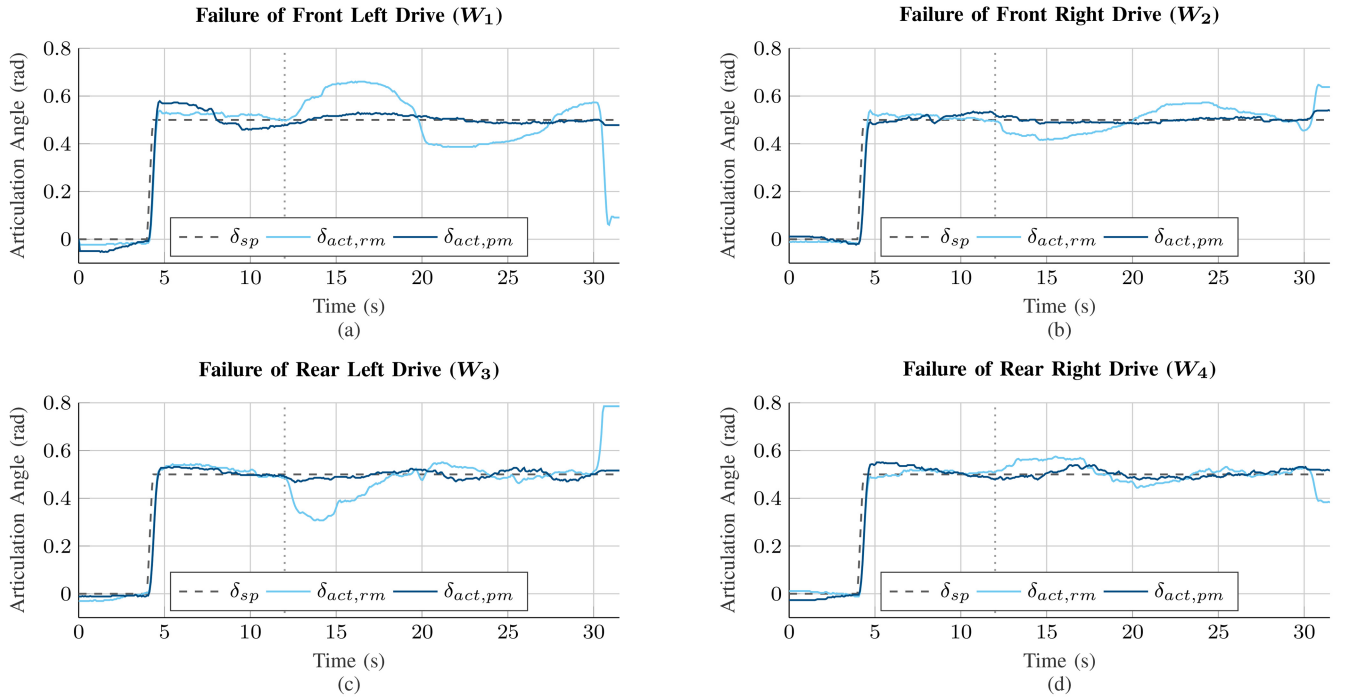


FIGURE 12. Comparison of sudden failures of different drives during the step-steer maneuver from the demonstrator vehicle test runs, respectively for the two attempts with reference control method (rm) and proposed control method (pm). The time of failure is indicated by dotted vertical line. (a) Test runs 3.1 and 3.2. (b) Test runs 4.1 and 4.2. (c) Test runs 5.1 and 5.2. (d) Test runs 6.1 and 6.2.

0.015 rad which corresponds to a change of -88% compared to the reference method. When the failure occurred, there was an immediate redistribution in which the drive torque M_{D_4} was increased and the drive torque M_{D_3} was slightly reduced. Intervention by the steering controller was not required, as can be seen from the unchanged course of the steering torque.

D. COMPARISON OF THE DRIVE FAILURES ON DIFFERENT WHEELS

Failures on different drives vary in terms of their effect on the course of the articulation angle when using the reference method. As can be seen from Fig. 12 and Table 2, with the reference method, a failure of a drive on one of the inner curve wheels of the demonstrator vehicle results in a larger maximum control error $\hat{\delta}_{error}$ (0.439 rad on W_1 and 0.285 rad on W_3) compared to a failure on the drives of the outer wheels (0.147 rad on W_2 and 0.117 rad on W_4).

In all failure cases the use of the proposed method leads to a reduction of the maximum control error $\hat{\delta}_{error}$ (-93% on W_1 , -72% on W_2 , -88% on W_3 , -67% on W_4) as well as the root-mean-square error δ_{RMSE} (-88% on W_1 , -78% on W_2 , -84% on W_3 , -60% on W_4).

To evaluate the performance of the failure compensation, we also compare the maximum deviation $\hat{\delta}_{error}$ in the failure cases with the maximum deviation in the failure-free case. We therefore use the maximum deviation of test run 1.1 as the reference value (0.039 rad). According to Table 2 in the test runs with the proposed method, a failure at the rear

right wheel resulted in the same deviation as the reference metric. The metric for a failure at the front right wheel is 5% larger, and at the front left wheel and rear left wheel the maximum deviation in the failure case is even smaller than that of the reference (-21% and -15% , respectively). It can be concluded that using the proposed method, the maximum deviation errors in all four failure cases do not differ significantly from the failure-free reference run and, on average, even lead to a better overall performance.

When defining the test plan (see Section II-C4), the focus of the analysis was on the failure of the front left drive when cornering to the left. This was done on the basis of findings from preliminary tests, which showed that the failure of the front left wheel in this driving situation represents the worst case. This finding can be confirmed from the results, since both $\hat{\delta}_{error}$ and δ_{RMSE} become maximum for the drive failure at wheel W_1 when using the reference method.

E. DRIVE FAILURE DURING DYNAMIC DRIVING MANEUVER (SLALOM)

The slalom maneuver test runs 7.1 and 7.2 were only conducted in simulation. Test drives with the demonstrator vehicle were not possible because the test site, which was chosen for its smooth surface in order to record measurement data without disturbance, did not offer the required length of about 27 m. The results are shown in Fig. 13. Before the failure, both the reference control method and the proposed control method followed the sinusoidal articulation angle setpoint with a time offset of 0.45 s and an

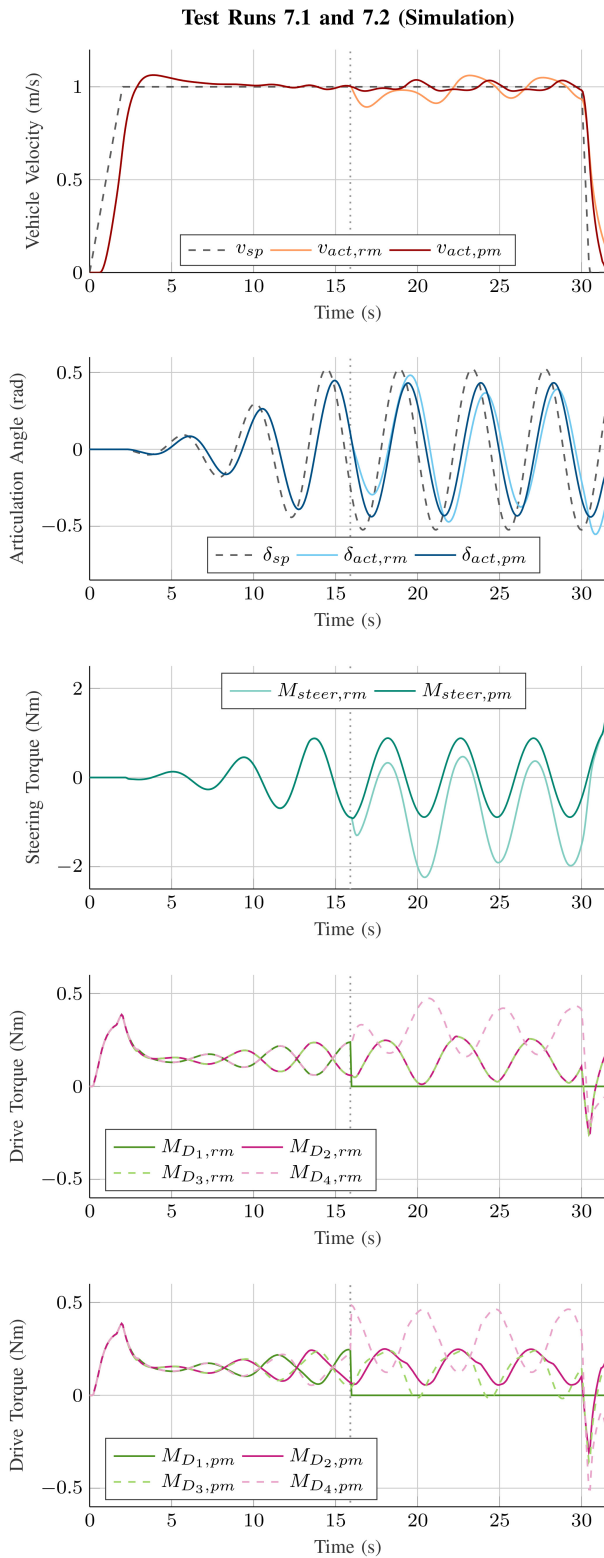


FIGURE 13. Results of the slalom maneuvers with sudden failure of the front left drive at $t = 15.9$ s (indicated by dotted vertical line) from the simulation test run (test runs 7.1 and 7.2), respectively for the two attempts with reference control method (rm) and proposed control method (pm).

amplitude reduction of 14%. At the moment of the highest steering torque the drive failure was initiated ($t = 15.9$ s). The reference method without active redistribution of the

drive torques after the failure led to an inconsistent amplitude of the resulting articulation angle curve and thus to an inaccurate vehicle guidance behavior. Again, the course of the articulation angle was not influenced by the actuator failure when the proposed control method was used. The steering torque output by the controller followed the same sinusoidal curve as before the failure. The curves of the resulting drive forces showed a periodic but no longer sinusoidal curve after the failure. This is due to the pseudo lever arms which constantly change with the articulation angle.

V. CONCLUSION

With the simulation model and demonstrator vehicle studies we could prove that the proposed control method can compensate for the failure of a drive motor of the four-wheel-drive articulated vehicle. After the drive failure the vehicle continued to follow the course of the set-points for articulation angle and velocity without negative influence at the same level as before, even in dynamic situations such as acceleration, deceleration or slalom driving. Our approach of a control allocation which we formulated as a constrained weighted least squares problem proved to be a suitable solution for the intended target. In failure-free operation the proposed controller approach can additionally use the available degrees of freedom of the drive torque distribution to achieve certain optimization objectives, which could be investigated in further research.

With the results we also could verify the validity of the used correlations in the control effectiveness matrix and the flexible pseudo lever arms.

The controllers for velocity and articulation angle, which precede the control allocation, were not the focus of this work and were implemented as simple PID controllers. The results showed that the guidance and disturbance behavior of the controller offers further potential for optimization, since control deviations occurred during the step-steer maneuver and especially during the slalom maneuver regardless of whether a drive has failed or not. Improvements could be achieved by alternative controller approaches such as cascaded PID controllers, gain-scheduled PID controllers, feedback linearization, linear-quadratic regulator or model predictive control.

For use in automated vehicles, not only fault-tolerant realization of the desired articulation angle is necessary, but also reliable path tracking. We consider our presented approach for a fault-tolerant vehicle dynamics controller as a prerequisite for the fault-tolerant functionality of a higher-level trajectory or path tracking controller. By reliably realizing the output variables of the path tracking controller, it can continue its functionality without being affected by a drive failure. Considering the behavior of a path tracking controller in combination with the proposed vehicle dynamics controller was not part of this work and should be investigated in further research.

TABLE 3. Vehicle model parameters and values for the demonstrator vehicle.

Parameter	Description	Value
$c_{1,2}$	Cornering stiffness front wheels	570 N/rad
$c_{3,4}$	Cornering stiffness rear wheels	600 N/rad
d	Torsional damping coefficient	0.85 Nm-s/rad
F_R	Wheel resistance force	2.237 N
I_1	Moment of inertia front section	0.201 kg-m ²
I_2	Moment of inertia rear section	0.226 kg-m ²
l_1	Distance front axle to articulation joint	0.26 m
l_2	Distance rear axle to articulation joint	0.26 m
l_{CG_1}	Distance front axle to CG_1	-0.02 m
l_{CG_2}	Distance rear axle to CG_2	0.025 m
m_1	Mass front section	8.670 kg
m_2	Mass rear section	9.765 kg
r_W	Dynamic wheel radius	0.0663 m
s_1	Track width front axle	0.33 m
s_2	Track width rear axle	0.33 m

For the integration of the proposed control method into the overall control structure of a steer-by-wire or automated vehicle, a failure detection will be needed (Fig. 6). This can be a diagnostic system within the individual control units of the drives or a central system that detects the errors by analyzing various vehicle sensors or the vehicle behavior.

Overall, we conclude that the proposed control approach is an appropriate solution in all respects to serve as a basis for further development of fault-tolerant drive-by-wire solutions for electrified articulated vehicles.

APPENDIX A DERIVATION OF SYSTEM EQUATIONS

This section describes the derivation of the system equation in detail and relates to Fig. 4. The vehicle parameters used in the model are described in Table 3 including the values identified for the demonstrator vehicle.

The position vectors from the center of gravity CG_1 of the front vehicle section to the contact point of the front wheels W_1 and W_2 and to the articulation joint J in coordinates of the front section coordinate system (index F) are found as

$$\begin{aligned} \mathbf{r}_{CG_1 \rightarrow W_1}^F &= [-l_{CG_1} \quad \frac{1}{2}s_1 \quad 0]^T \\ \mathbf{r}_{CG_1 \rightarrow W_2}^F &= [-l_{CG_1} \quad -\frac{1}{2}s_1 \quad 0]^T \\ \mathbf{r}_{CG_1 \rightarrow J}^F &= [-l_{CG_1} - l_1 \quad 0 \quad 0]^T \end{aligned} \quad (24)$$

Similarly, the vectors from CG_2 to the rear wheels and the articulated joint can be found in coordinates of the rear section coordinate system as

$$\begin{aligned} \mathbf{r}_{CG_2 \rightarrow W_3}^R &= [l_{CG_2} \quad \frac{1}{2}s_2 \quad 0]^T \\ \mathbf{r}_{CG_2 \rightarrow W_4}^R &= [l_{CG_2} \quad -\frac{1}{2}s_2 \quad 0]^T \\ \mathbf{r}_{CG_2 \rightarrow J}^R &= [l_{CG_2} + l_2 \quad 0 \quad 0]^T \end{aligned} \quad (25)$$

With the rotation matrix

$$\mathbf{R}^{R \rightarrow F} = \begin{bmatrix} \cos(\delta) & \sin(\delta) & 0 \\ -\sin(\delta) & \cos(\delta) & 0 \\ 0 & 0 & 1 \end{bmatrix} \quad (26)$$

the vectors with rear section coordinates (index R) are transformed into the front section coordinate system:

$$\begin{aligned} \mathbf{r}_{CG_2 \rightarrow W_3}^F &= \mathbf{R}^{R \rightarrow F} \mathbf{r}_{CG_2 \rightarrow W_3}^R \\ \mathbf{r}_{CG_2 \rightarrow W_4}^F &= \mathbf{R}^{R \rightarrow F} \mathbf{r}_{CG_2 \rightarrow W_4}^R \\ \mathbf{r}_{CG_2 \rightarrow J}^F &= \mathbf{R}^{R \rightarrow F} \mathbf{r}_{CG_2 \rightarrow J}^R \end{aligned} \quad (27)$$

For angular velocity and angular acceleration of CG_1 applies:

$$\begin{aligned} \boldsymbol{\omega}_{CG_1}^F &= [0 \quad 0 \quad \dot{\psi}_1]^T \\ \boldsymbol{\alpha}_{CG_1}^F &= \frac{d}{dt} \boldsymbol{\omega}_{CG_1}^F = [0 \quad 0 \quad \ddot{\psi}_1]^T \end{aligned} \quad (28)$$

And for CG_2 we get

$$\boldsymbol{\omega}_{CG_2}^F = [0 \quad 0 \quad \dot{\psi}_2]^T = [0 \quad 0 \quad \dot{\psi}_1 - \dot{\delta}]^T \quad (29)$$

and

$$\boldsymbol{\alpha}_{CG_2}^F = \frac{d}{dt} \boldsymbol{\omega}_{CG_2}^F = [0 \quad 0 \quad \ddot{\psi}_2]^T = [0 \quad 0 \quad \ddot{\psi}_1 - \ddot{\delta}]^T \quad (30)$$

The velocity of CG_1 is found as

$$\mathbf{v}_{CG_1}^F = [\dot{x}_1 \quad \dot{y}_1 \quad 0]^T \quad (31)$$

The acceleration is determined by deriving the velocity vector. It should be noted that the basis vectors are taken into account in the derivation, since they change their orientation with the vehicle. For CG_1 we get:

$$\mathbf{a}_{CG_1}^F = [\ddot{x}_1 - \dot{y}_1 \dot{\psi}_1 \quad \ddot{y}_1 + \dot{x}_1 \dot{\psi}_1 \quad 0]^T \quad (32)$$

The velocity vector of CG_2 can be calculated via an intermediate step by considering the velocity \mathbf{v}_J^F of the articulated joint J . With (31), (28) and (24) we find

$$\mathbf{v}_J^F = \mathbf{v}_{CG_1}^F + \boldsymbol{\omega}_{CG_1}^F \times \mathbf{r}_{CG_1 \rightarrow J}^F \quad (33)$$

With the position vector from J to CG_2 and the rotational velocity of CG_2 (29) we first get

$$\mathbf{v}_{CG_2}^F = \mathbf{v}_J^F + \boldsymbol{\omega}_{CG_2}^F \times \mathbf{r}_{J \rightarrow CG_2}^F \quad (34)$$

and finally

$$\begin{aligned} \mathbf{v}_{CG_2}^F &= \mathbf{v}_{CG_1}^F + \boldsymbol{\omega}_{CG_1}^F \times \mathbf{r}_{CG_1 \rightarrow J}^F \\ &\quad + \boldsymbol{\omega}_{CG_2}^F \times (-\mathbf{r}_{CG_2 \rightarrow J}^F) \end{aligned} \quad (35)$$

The derivation of (33) results in

$$\begin{aligned} \mathbf{a}_J^F &= \mathbf{a}_{CG_1}^F + \boldsymbol{\omega}_{CG_1}^F \times (\boldsymbol{\omega}_{CG_1}^F \times \mathbf{r}_{CG_1 \rightarrow J}^F) \\ &\quad + \boldsymbol{\alpha}_{CG_1}^F \times \mathbf{r}_{CG_1 \rightarrow J}^F \end{aligned} \quad (36)$$

With (34) and (36) the acceleration of CG_2 is given as

$$\begin{aligned} \mathbf{a}_{CG_2}^F &= \mathbf{a}_J^F + \boldsymbol{\omega}_{CG_2}^F \times (\boldsymbol{\omega}_{CG_2}^F \times (-\mathbf{r}_{CG_2 \rightarrow J}^F)) \\ &\quad + \boldsymbol{\alpha}_{CG_2}^F \times (-\mathbf{r}_{CG_2 \rightarrow J}^F) \end{aligned} \quad (37)$$

The velocities at the positions of the wheels are derived analogously and result in:

$$\begin{aligned} \mathbf{v}_{W_1}^F &= \mathbf{v}_{CG_1}^F + \boldsymbol{\omega}_{CG_1}^F \times \mathbf{r}_{CG_1 \rightarrow W_1}^F \\ \mathbf{v}_{W_2}^F &= \mathbf{v}_{CG_1}^F + \boldsymbol{\omega}_{CG_1}^F \times \mathbf{r}_{CG_1 \rightarrow W_2}^F \end{aligned}$$

$$\begin{aligned} \mathbf{v}_{W_3}^F &= \mathbf{v}_{CG_2}^F + \boldsymbol{\omega}_{CG_2}^F \times \mathbf{r}_{CG_2 \rightarrow W_3}^F \\ \mathbf{v}_{W_4}^F &= \mathbf{v}_{CG_2}^F + \boldsymbol{\omega}_{CG_2}^F \times \mathbf{r}_{CG_2 \rightarrow W_4}^F \end{aligned} \quad (38)$$

The slip angles are calculated from the components of the velocity vectors of the wheels as follows:

$$\alpha = \arctan\left(\frac{v_y}{v_x}\right) \quad (39)$$

The components of the velocity vectors of the wheels can be found as

$$\begin{aligned} v_{W_i,x} &= [1 \quad 0 \quad 0] \mathbf{v}_{W_i} \\ v_{W_i,y} &= [0 \quad 1 \quad 0] \mathbf{v}_{W_i} \end{aligned} \quad (40)$$

For the calculation of the slip angles at the rear wheels, the velocity vectors (38) must be described in the coordinate system of the rear section:

$$\begin{aligned} \mathbf{v}_{W_3}^R &= (\mathbf{R}^{R \rightarrow F})^{-1} \mathbf{v}_{W_3}^F \\ \mathbf{v}_{W_4}^R &= (\mathbf{R}^{R \rightarrow F})^{-1} \mathbf{v}_{W_4}^F \end{aligned} \quad (41)$$

We finally get the slip angles as

$$\begin{aligned} \alpha_1 &= \arctan\left(\frac{v_{W_1,y}^F}{|v_{W_1,x}^F|}\right) \\ \alpha_2 &= \arctan\left(\frac{v_{W_2,y}^F}{|v_{W_2,x}^F|}\right) \\ \alpha_3 &= \arctan\left(\frac{v_{W_3,y}^R}{|v_{W_3,x}^R|}\right) \\ \alpha_4 &= \arctan\left(\frac{v_{W_4,y}^R}{|v_{W_4,x}^R|}\right) \end{aligned} \quad (42)$$

The forces derived from the free body diagram (Fig. 4) can now be expressed vectorially.

The wheel forces and joint forces of the front section become

$$\begin{aligned} \mathbf{F}_{W_1}^F &= [F_{D_1} - F_R \operatorname{sgn}(v_{W_1,x}^F) \quad -c_{1,2}\alpha_1 \quad 0]^T \\ \mathbf{F}_{W_2}^F &= [F_{D_2} - F_R \operatorname{sgn}(v_{W_2,x}^F) \quad -c_{1,2}\alpha_2 \quad 0]^T \\ \mathbf{R}^F &= [R_x \quad R_y \quad 0]^T \end{aligned} \quad (43)$$

And the wheel forces of the rear section can be found as

$$\begin{aligned} \mathbf{F}_{W_3}^R &= \mathbf{R}^{R \rightarrow F} \mathbf{F}_{W_3}^F \\ &= \mathbf{R}^{R \rightarrow F} \begin{bmatrix} F_{D_3} - F_R \operatorname{sgn}(v_{W_3,x}^F) \\ -c_{3,4}\alpha_3 \\ 0 \end{bmatrix} \\ \mathbf{F}_{W_4}^R &= \mathbf{R}^{R \rightarrow F} \mathbf{F}_{W_4}^F \\ &= \mathbf{R}^{R \rightarrow F} \begin{bmatrix} F_{D_4} - F_R \operatorname{sgn}(v_{W_4,x}^F) \\ -c_{3,4}\alpha_4 \\ 0 \end{bmatrix} \end{aligned} \quad (44)$$

Since the slip angles have a singularity when the vehicle is standing still, the F_y component of the wheel force vectors have to be set to 0 in this case.

\mathbf{M}_D^F is the damping torque that includes friction in the articulation joint and effects that occur in the wheel contact while pivoting. Using the angular velocities from equation (28) and (29), the damping factor d results in

$$\mathbf{M}_D^F = d(\boldsymbol{\omega}_{CG_1}^F - \boldsymbol{\omega}_{CG_2}^F) \quad (45)$$

From the acceleration (32) and the forces (43) follows the equilibrium of forces of the front section:

$$m_1 \mathbf{a}_{CG_1}^F = \mathbf{F}_{W_1}^F + \mathbf{F}_{W_2}^F + \mathbf{R}^F \quad (46)$$

From the angular acceleration (32) and the forces (43) with the corresponding lever arms (24) as well as the moment vector (45) follows the moment equilibrium of the front section:

$$\begin{aligned} I_1 \boldsymbol{\alpha}_{CG_1}^F &= \mathbf{r}_{CG_1 \rightarrow W_1} \times \mathbf{F}_{W_1}^F + \mathbf{r}_{CG_1 \rightarrow W_2} \times \mathbf{F}_{W_2}^F \\ &\quad + \mathbf{r}_{CG_1 \rightarrow J} \times \mathbf{R}^F - \mathbf{M}_D^F \end{aligned} \quad (47)$$

From the acceleration (37) and the forces (44) follows the equilibrium of forces of the rear section:

$$m_2 \mathbf{a}_{CG_2}^F = \mathbf{F}_{W_3}^F + \mathbf{F}_{W_4}^F - \mathbf{R}^F \quad (48)$$

From the angular acceleration (37) and the forces (44) with the corresponding lever arms (25) as well as the moment vector (45) follows the moment equilibrium of the rear section:

$$\begin{aligned} I_2 \boldsymbol{\alpha}_{CG_2}^F &= \mathbf{r}_{CG_2 \rightarrow W_3} \times \mathbf{F}_{W_3}^F + \mathbf{r}_{CG_2 \rightarrow W_4} \times \mathbf{F}_{W_4}^F \\ &\quad - \mathbf{r}_{CG_2 \rightarrow J} \times \mathbf{R}^F + \mathbf{M}_d^F \end{aligned} \quad (49)$$

APPENDIX B DERIVATION OF PSEUDO STEERING LEVER ARMS

The pseudo steering lever arms r_{S_i} have to be found so that

$$M_{Steer} = -F_{D_1} r_{S_1} + F_{D_2} r_{S_2} + F_{D_3} r_{S_3} - F_{D_4} r_{S_4} \quad (50)$$

is the sum of the torques that the driving forces generate about the articulation joint axis. Not only the direct effect of the respective driving force on M_{Steer} must be taken into account, but also the indirect effect caused by lateral axis force components (F_{y_f} , F_{y_r}) resulting from the driving force. For derivation, the static free body diagram shown in Fig. 14 is considered. It does not contain any dynamic forces or moments, since only the effect of the forces that can be directly influenced by the controller output is relevant here. All other influences causing the pivoting of the vehicle sections, such as the dynamic lateral wheel forces or inertial forces, act as counterforces, that the controller is supposed to compensate for by specifying M_{Steer} .

Accordingly M_{Steer} results from the free body diagram as

$$\begin{aligned} M_{Steer} &= (-F_{D_1} + F_{D_2} + F_{D_3} - F_{D_4}) \frac{1}{2} s \\ &\quad + (F_{y_f} + F_{y_r}) l \end{aligned} \quad (51)$$

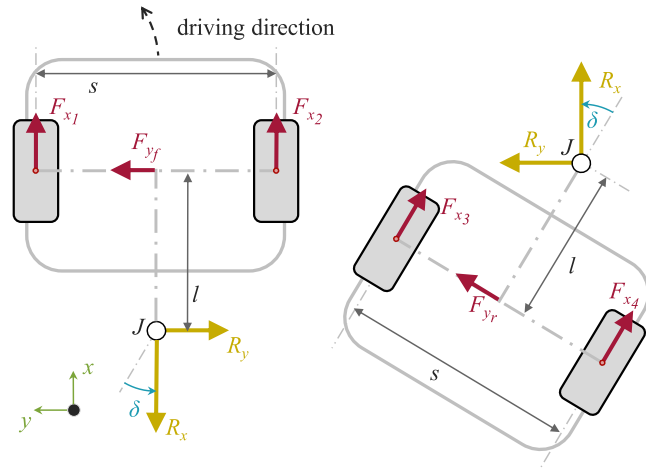


FIGURE 14. Static free body diagram for derivation of lateral axis forces F_{yf} , F_{yr} induced by driving forces F_{D1} – F_{D4} .

The four equilibria of forces, one in x and one in y direction per vehicle section can be found as

$$\begin{aligned} 0 &= F_{x1} + F_{x2} - R_x \\ 0 &= F_{yf} - R_y \\ 0 &= R_x + \cos(\delta)(F_{x3} + F_{x4}) + \sin(\delta)F_{yr} \\ 0 &= R_y + \cos(\delta)F_{yr} - \sin(\delta)(F_{x3} + F_{x4}) \end{aligned} \quad (52)$$

By resolving for $F_{yf} + F_{yr}$ we get

$$F_{yf} + F_{yr} = (-F_{D1} - F_{D2} + F_{D3} + F_{D4}) \tan\left(\frac{1}{2}\delta\right) \quad (53)$$

Finally, with (51) M_{Steer} becomes

$$\begin{aligned} M_{Steer} &= -F_{D1} \underbrace{\left(\frac{1}{2}s + l \tan\left(\frac{1}{2}\delta\right)\right)}_{r_{S1}=r_{Sl}} \\ &+ F_{D2} \underbrace{\left(\frac{1}{2}s - l \tan\left(\frac{1}{2}\delta\right)\right)}_{r_{S2}=r_{Sr}} \\ &+ F_{D3} \underbrace{\left(\frac{1}{2}s + l \tan\left(\frac{1}{2}\delta\right)\right)}_{r_{S3}=r_{Sl}} \\ &- F_{D4} \underbrace{\left(\frac{1}{2}s - l \tan\left(\frac{1}{2}\delta\right)\right)}_{r_{S4}=r_{Sr}} \end{aligned} \quad (54)$$

It can be seen that the pseudo steering lever arms are identical on one side of the vehicle each. On the inside of the curve, they increase as the articulation angle increases, while on the outside of the curve they decrease to the same extent. For the dimensions of the demonstration vehicle, they become 0.165 m for $\delta = 0^\circ$ and change to 0.286 m and 0.044 m, respectively, at the maximum articulation angle.

ACKNOWLEDGMENT

Many thanks to Luca Wahl and Clemens Brauch for their contribution in modifying and commissioning the demonstrator vehicle and in performing the simulation and vehicle test runs. The authors acknowledge support by the KIT-Publication Fund of the Karlsruhe Institute of Technology.

REFERENCES

- [1] A. Jentzsch, J. Janda, G. Xu, P. Wiedenhoff, and A. Girisch. "The future of commercial vehicles: How new technologies are transforming the industry." Accessed: Mar. 3, 2021. [Online]. Available: <https://www.bcg.com/de-de/publications/2019/future-commercial-vehicles>
- [2] R. Budich, "Untersuchungen zum Einsatz von Elektrokleinkehrmaschinen als Beitrag zur Dekarbonisierung des kommunalen Verkehrs," Ph.D. dissertation, Technische Universität Dresden, Fakultät Verkehrswissenschaften, Dresden, Germany, 2019.
- [3] J. Jeon et al., "Autonomous robotic street sweeping: Initial attempt for curbside sweeping," in *Proc. IEEE Int. Conf. Robot. Automat.*, 2017, pp. 72–73.
- [4] C. Altafani, "Why to use an articulated vehicle in underground mining operations?" in *Proc. IEEE Int. Conf. Robot. Automat.*, May 1999, pp. 3020–3025.
- [5] T. Nayl, "On autonomous articulated vehicles," Ph.D. dissertation, Dept. Comput. Sci., Elect. Space Eng., Luleå Univ. Technol., Luleå, Sweden, 2015.
- [6] A. Druckner, R. Stroph, and P. Pfeffer, "Drive-by-wire," in *Handbook of Intelligent Vehicles*, A. Eskandarian, Ed. London, U.K.: Springer, 2012, pp. 235–282.
- [7] J. Becker, M. Helmle, and O. Pink, "System architecture and safety requirements for automated driving," in *Automated Driving*, D. Watzenig and M. Horn, Eds. Cham, Switzerland: Springer Int., 2017, pp. 265–283.
- [8] C. Huang, F. Naghdy, H. Du, and H. Huang, "Fault tolerant steer-by-wire systems: An overview," *Annu. Rev. Control*, vol. 47, pp. 98–111, Apr. 2019.
- [9] P. J. Bergmiller, *Towards Functional Safety in Drive-by-Wire Vehicles*. Cham, Switzerland: Springer Int., 2015.
- [10] J. Wadehul, D. Engelmann, P. Kautzmann, and J. Römer, "Development of a novel steering concept for articulated vehicles," *ATZ Offhighw. Worldwide*, vol. 11, no. 4, pp. 54–61, 2018.
- [11] Y. He, A. Khajepour, J. McPhee, and X. Wang, "Dynamic modelling and stability analysis of articulated frame steer vehicles," *Int. J. Heavy Veh. Syst.*, vol. 12, no. 1, pp. 28–59, 2005.
- [12] J. Chun, W. Ping, S. Yanhua, and J. B. Michael, "Differential control strategy based on an equal slip rate for an all-wheel electricdrive underground articulated dumping truck," *J. Eng. Sci. Technol. Rev.*, vol. 7, no. 4, pp. 163–168, 2014.
- [13] T. Xu, X. Ji, C. Fei, Y. Liu, and Y. Shen, "Research on assist-steering method for distributed-drive articulated heavy vehicle based on the co-simulation model," SAE Int., Warrendale, PA, USA, 2020.
- [14] *Road Vehicles—Lateral Transient Response Test Methods—Open-Loop Test Methods*, Int. Org. Standard., London, U.K., ISO 7401:2011, 2011.
- [15] B. Siciliano and O. Khatib, *Springer Handbook of Robotics*. Cham, Switzerland: Springer Int., 2016.
- [16] M. W. Oppenheimer, D. B. Doman, and M. A. Bolender, "Control allocation for over-actuated systems," in *Proc. 14th Mediterranean Conf. Control Automat.*, 2006, pp. 1–6.
- [17] O. Härkegård, "Efficient active set algorithms for solving constrained least squares problems in aircraft control allocation," in *Proc. 41st IEEE Conf. Decis. Control*, 2002, pp. 1295–1300.
- [18] MathWorks. "Solve systems of linear equations $ax = B$ for x - MATLAB `mldivide \`." Accessed: Mar. 21, 2022. [Online]. Available: <https://www.mathworks.com/help/matlab/ref/mldivide.html>
- [19] A. Seiffer, C. Brauch, N. Schmidt, and C. Haschke. "Failure-compensating control method for a four-wheel independently driven articulated vehicle." Feb.–May 2022. [Online]. Available: <https://doi.org/10.5445/IR/1000143340>
- [20] Colliseum. "Lenkübersetzung-angaben der hersteller." Accessed: Nov. 6, 2022. [Online]. Available: <https://www.colliseum.eu/wiki/index.php?title=Lenk%C3%BCbersetzung&oldid=30369>



ALEXANDER SEIFFER received the M.Sc. degree in mechanical engineering from the Karlsruhe Institute of Technology (KIT), Karlsruhe, Germany, in 2015, where he is currently pursuing the Doctoral degree with the Working Group Automated Mobility, SHARE at KIT (Schaeffler Hub for Advanced Research at Karlsruhe Institute of Technology) under the supervision of F. Gauterin. Since 2015, he has been working with Schaeffler Technologies AG & Co. KG. His research interests include automated driving,

technical reliability and resilience, vehicle dynamics, and over-actuated vehicles.



LUKAS SCHÜTZ received the M.Sc. degree in mechanical engineering from the Karlsruhe Institute of Technology (KIT), Karlsruhe, Germany, in 2019. He worked as a working student with the Working Group Automated Mobility, SHARE at KIT (Schaeffler Hub for Advanced Research at Karlsruhe Institute of Technology) from 2017 to 2019. Since 2019, he has been working with Knorr-Bremse Systeme für Nutzfahrzeuge GmbH as a Engineer of Vehicle Dynamics Control and Redundancy for Automated Driving.



MICHAEL FREY received the Diploma and Doctoral degrees in mechanical engineering from the University of Karlsruhe in 1993 and 2004, respectively. He is the Manager of the Research Group Automation and the Research Group Suspension and Propulsion Systems, Institute of Vehicle System Technology. His research interests are autonomous driving, driver assistance systems, operational strategies, suspension systems, vehicle dynamics, as well as vehicle modeling and optimization.



FRANK GAUTERIN received the Diploma degree in physics from the University of Münster, Germany, in 1989, and the Dr.rer.nat. (Ph.D.) degree from the University of Oldenburg, Germany, in 1994. From 1989 to 2000, he worked as an Acoustics Engineer and from 2000 to 2006 as the Director of the Noise Vibration and Harshness (NVH) Engineering Profit Centre, Continental AG, Hanover, Germany, with locations in Germany, USA, and Malaysia. Since 2006, he has been a Full Professor of Vehicle Technology with the Karlsruhe Institute of

Technology (KIT), Germany, the Head of the Institute of Vehicle System Technology, and a Scientific Spokesperson, KIT Centre Mobility Systems. His research interests are vehicle conception, control, suspension and drive systems, tire road interaction, and NVH.